Hindawi
International Journal of Photoenergy
Volume 2019, Article ID 5372904, 9 pages
https://doi.org/10.1155/2019/5372904

Research Article

Photovoltaic and Physical Characteristics of Screen-Printed Monocrystalline Silicon Solar Cells with Laser Doping and Electroplated Copper

Chin-Lung Cheng, Chi-Chung Liu, and Chun-Tin Yeh

Department of Electro-Optical Engineering, National Formosa University, Yunlin 63201, Taiwan

Correspondence should be addressed to Chin-Lung Cheng; chengcl@nfu.edu.tw

Received 17 September 2018; Accepted 15 November 2018; Published 31 January 2019

Academic Editor: Jegadesan Subbiah

Photovoltaic and physical characteristics of screen-printed monocrystalline silicon solar cells (SPMSCs) were presented with electroplated copper (EPC) as the rear contact. The boron back surface field (B-BSF) formed by spin-on doping and laser doping (LD) was prepared as a seed layer for the EPC. The LD parameters, including the laser focus, laser power, laser speed, and laser line pitch, were investigated. Moreover, the effects of KOH etching on the surface properties after the LD process were explored. Furthermore, to enhance the adhesion between the B-BSF seed layer and EPC contact layer, a laser pinhole process was proposed. Finally, the EPC processes with various electroplating times were addressed. The results revealed that the mechanism of enhancements could be attributed to a continuous B-BSF seed layer and a reduction of series resistance, as well as an increase of open-circuit voltage and adhesion between the B-BSF seed layer and EPC contact layer.

1. Introduction

Screen-printed mono- and multicrystalline silicon solar cells have been extensively developed for industrial solar cells [1–4]. In general, screen-printed Al pastes were utilized on SPMSCs for the rear contact [5–7]. The literature has reported that contact loss, which limits the conversion efficiency of solar cells, is one of the loss mechanisms [8]. Therefore, improvements in the bulk properties of a metal contact with low resistivity are highly desirable. Recently, electroplating technology has attracted considerable attention due to its low resistivity and low-cost metallization [9]. There are reports from the literature that performance can be enhanced by electroplating techniques. A one-step annealing front metal contact process by an adapted plating stack of Ni–Cu–Ag was investigated to enhance the spectral response of silicon-based solar cells [10]. Ni plating on a lightly doped emitter through SiN_x dielectric plus NiSi formation followed by Cu or Ag plating was used to balance the contact resistance and improve blue response of SPMSCs [11]. The implementation of a lightly doped emitter and plated Ni–Ag front side contacts was demonstrated to increase the conversion efficiency of silicon solar cells [12]. Improved photovoltaic characteristics for SPMSCs were demonstrated by EPC as the rear metallization. The seed layer for EPC was achieved by an Al back surface field formed by a screen-printed Al paste [13]. In this work, a B-BSF seed layer for EPC will be demonstrated.

Moreover, laser doping was widely adopted to form a selective emitter and rear contact for SPMSCs. For instance, two different approaches to form Cu-plated contacts based on the laser ablation of a SiN_x:H antireflection coating were achieved [14]. Investigations of a selective emitter in a single-step diffusion process for plated Ni-Cu metallization of crystalline silicon solar cells were demonstrated [15]. The influence of the laser power on the solar cell electrical parameters to ascertain the relationship and tradeoff between surface roughness and electrical performance was examined [16, 17]. Thus, in this work, a B-BSF layer formed by spin-on-dopant and LD technology was proposed as a seed layer for the EPC. Improved conversion efficiency for SPMSCs will be demonstrated by EPC as the rear contact.

2. Experimental Methods

To explore the effects of LD as a seed layer for EPC on the photovoltaic and physical characteristics of SPMSCs, square samples ($156 \times 156\,mm^2$) of (100)-oriented p-type silicon wafers with 0.5–3 Ω·cm and $200 \pm 20\,\mu m$ were prepared. Alkali texturing was performed in a solution of 1.73% KOH at 83°C for 10 min. The front emitters of the p-type silicon substrates were formed by phosphorus diffusion at 850°C. After single-side edge isolation and PSG etching, the sheet resistances of the front emitters were approximately $100 \pm 5\,\Omega$/sq. For passivation and antireflection coating, a standard SiN_x film with a thickness of 80 nm was deposited on the n^+ emitters by the decomposition of NH_3 and SiH_4 using plasma-enhanced chemical vapor deposition at a frequency of 13.56 MHz. Directly, a Ag front paste was screen printed on the front side of SPMSCs and dried in an infrared belt furnace at 230°C. Then, an industrial infrared belt furnace was used to fire Ag pastes into n-type emitters. The peak temperature and belt speed were set at 790°C and 508 cm/min, respectively. Next, to protect the front contact of SPMSCs, a polymer paste was spin cast onto the front surface of SPMSCs at 3000 rpm and dried at 130°C for 30 min. After the protection process, a boron paste (Futurrex Inc., USA, Boron Dopant Coating BDC5-25001) was spun onto the rear side of SPMSCs. LD processes were formed by a Nd:YAG solid laser with a wavelength of 1064 nm on the rear side of SPMSCs. The parameters of the laser positions from the focus were tuned from −012 to 0.08 mm. The negative value indicates that the laser-treated surface was below the laser focus. The laser powers were addressed from 0.6 to 1.6 W. The laser speeds were achieved from 240 to 560 mm/min. The laser line pitches ranged from 10 to 50 μm. To enhance the adhesion between the B-BSF seed layer and EPC contact layer, a laser pinhole after the LD process was proposed. The laser pinhole process was achieved at a laser power of 2.6 W and a laser contact spacing of 600 μm. After all LD processes, alkali etching ranging from 0 to 60 s was performed in a solution of 1.73% KOH at 83°C. Finally, various EPC times were addressed from 20 to 70 min. The current density of the EPC was addressed at $25\,mA/cm^2$. A SPMSC with a screen-printed Al rear was fabricated as a reference. The current density–voltage curves of SPMSCs were measured under standard test conditions (AM1.5G spectrum, $100\,mW/cm^2$, and 25°C). The conversion efficiency was an average of all the measurements over 25 devices, with an error bar. Surface morphologies were examined by field emission scanning electron microscopy (FESEM). The peeling force test was utilized at a constant speed of 1 mm/s at a constant angle of 90° between the cell and ribbon with a $20 \pm 5\,\mu m$ layer of Sn62Pb36Ag2.

3. Results and Discussion

Figure 1 presents various conversion efficiencies of SPMSCs with the B-BSF seed layer and EPC contact layer as the rear contacts. The LD processes were treated at various positions from the laser focus. The results suggested that an optimum condition was achieved at −0.04 mm from the laser focus rather than at the laser focus. The −0.04 mm position indicates that the laser beam focused at 0.04 mm above the surface. It has been reported that the strongest spallation effect was obtained when the focus of the laser beam was located into the bulk substrate [18]. The laser focus position strongly affects the grade of the laser-induced spallation. Moreover, improved conversion efficiency can be demonstrated by a careful tailoring of the beam profile [19]. Thus, a B-BSF seed layer formed at −0.04 mm from laser focus was prepared for EPC as the rear contact of SPMSCs. The achievement of a conversion efficiency improvement of more than 2.9% absolute from 12.7% to 15.6% for SPMSCs with a tuning laser position from the laser focus was explored.

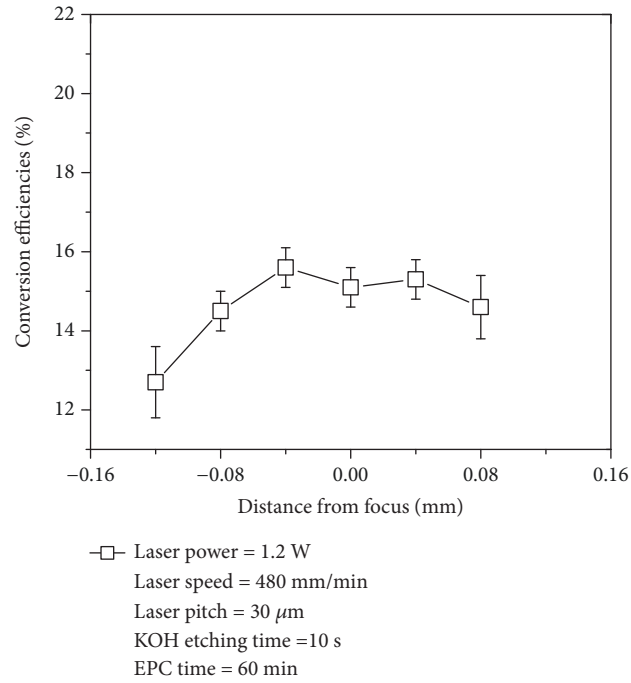

Figure 1: Conversion efficiency vs. laser position curve of SPMSCs with a B-BSF seed layer and EPC contact layer as the rear contacts.

To investigate the effects of various laser powers on the photovoltaic characteristics of SPMSCs, various conversion efficiencies of SPMSCs with the B-BSF seed layer and EPC contact layer as the rear contacts are shown in Figure 2. The results show that the conversion efficiency increases as the laser power is increased, until an optimum power is reached. Above this optimum power, the conversion efficiency decreases as the scanning power is increased. It has been reported that the conversion efficiency is reduced with an increase in diode current [16]. Thus, a B-BSF layer with a large amount of laser energy was demonstrated at a higher laser power. An optimum condition was achieved at a laser power of 1 W. The achievement of a conversion efficiency improvement of more than 4.3% absolute from 11.5% to 15.8% for SPMSCs with a tuning laser power was explored.

To demonstrate the mechanism of various laser powers on the surface properties after the LD process, FESEM surface morphology images of backside surfaces of SPMSCs with various laser powers of (a) 0.8, (b) 1.0, (c) 1.2, and (d) 1.4 W

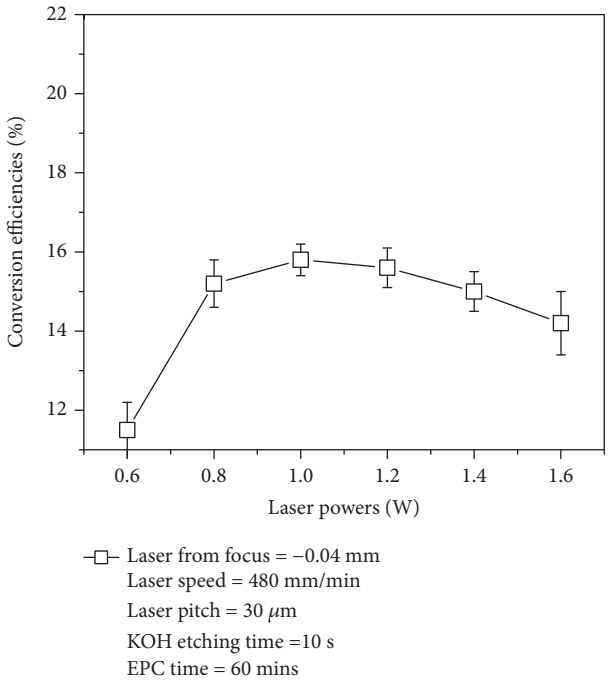

Figure 2: Conversion efficiency vs. laser power curve of SPMSCs with a B-BSF seed layer and EPC contact layer as the rear contacts.

are shown in Figure 3. The B-BSF seed layer was discontinuous for the laser power at 0.8 W, as shown in Figure 3(a). It has been reported that a greater dislocation appeared underneath the ablated region when the irradiation energy was increased [20]. The laser energy increases with increasing laser powers. Thus, the texturing pyramid disappeared at a laser power of 1.4 W, as shown in Figure 3(d). A suitable B-BSF seed layer was presented at a laser power of 1.0 W, as shown in Figure 3(b). Thus, a continuous B-BSF seed layer with low laser energy formed at a laser power of 1 W was prepared as a seed layer for the EPC contact layer.

To explore the effects of various laser speeds on the photovoltaic characteristics of SPMSCs, various conversion efficiencies of SPMSCs with the B-BSF seed layer and EPC contact layer as the rear contacts are shown in Figure 4. The results show a reduction in conversion efficiency at both slow and fast laser speeds. An optimum condition was achieved at a laser speed of 400 mm/min. The achievement of a conversion efficiency improvement of more than 2.5% absolute from 13.5% to 16.0% for SPMSCs with a tuning laser speed was explored.

To understand the mechanisms of various laser speeds on the surface properties of SPMSCs, various FESEM surface morphology images of backside surfaces of SPMSCs with various laser speeds of (a) 320, (b) 400, (c) 480, and (d) 560 mm/min are shown in Figure 5. It has been reported that the laser energy (J/cm^2) is related with the melting time [21]. Moreover, decreasing the scanning speed increases the melting time [16]. Thus, under a slow laser speed, more laser energy could be accumulated. A large amount of laser energy was formed at a slow laser speed. Therefore, a deep B-BSF seed layer could be formed at a slow laser speed, as shown in Figure 5(a). On the other hand, a discontinuous B-BSF seed layer was presented at a fast laser speed, as shown in Figures 5(c) and 5(d). The results reveal that a continuous B-BSF seed layer was addressed below 400 mm/min. Thus, a suitable laser speed was presented at 400 mm/min, as shown in Figure 5(b).

To examine the effects of various laser line pitches on the conversion efficiencies of SPMSCs with the B-BSF seed layer and EPC contact layer as the rear contacts, the conversion efficiency vs. laser line pitch curve is shown in Figure 6. The results show that the conversion efficiency increases as the laser line pitch is increased, until an optimum line pitch is reached. Above this optimum line pitch, the conversion efficiency decreases as the scanning line pitch is increased. It has been reported that diagonal cracks were observed in a laser doped with increasing doping overlaps [22]. An optimum condition was achieved at a laser line pitch of 30 μm. The achievement of a conversion efficiency improvement of more than 1.6% absolute from 14.6% to 16.2% for SPMSCs with a tuning laser line pitch was explored.

Figure 7 shows various FESEM surface morphology images of backside surfaces of SPMSCs with various laser line pitches of (a) 10 and (b) 40 μm. The width of the laser beam was measured to be approximately 12.6 μm, as shown in Figure 7(b). The results reveal that a continuous B-BSF seed layer was presented at a laser line pitch of 10 μm. Although a continuous B-BSF seed layer was addressed at a laser line pitch of 10 μm, the laser energy could be increased because the laser beams overlap each other [22]. Thus, the electroplating time for EPC can be reduced by a continuous B-BSF seed layer. On the contrary, a broken EPC contact layer could be formed at large laser line pitch. This could be due to a large spacing between the B-BSF seed layer regions. Therefore, the thicknesses of the EPC decrease with increasing laser line pitches (the thickness of the EPC will be demonstrated in the following discussion). Thus, a broken EPC contact layer could occur at a large laser line pitch under the same EPC time. A suitable laser line pitch was presented at 30 μm in this work.

Figure 8 shows the conversion efficiency vs. KOH etching time curve of SPMSCs with a B-BSF seed layer and EPC contact layer as the rear contacts. After the LD process, alkali etching ranging from 0 to 60 s was performed. The results show a decrease in conversion efficiency at both short and long KOH etching times. The conversion efficiency increases as the KOH etching time is increased, until an optimum time is reached. An optimum condition was achieved at a KOH etching time of 30 s. The achievement of a conversion efficiency improvement of more than 2.3% absolute from 14.1% to 16.4% for SPMSCs with a tuning KOH etching time was explored.

To understand the mechanism of enhancements, various FESEM surface morphology images of the backside surfaces of SPMSCs with various KOH etching times of (a) 30 and (b) 40 s are shown in Figure 9. It has been reported that laser damage can be removed by a KOH solution [20, 23]. A continuous B-BSF seed layer with large laser damage will be formed without KOH treatment. The results reveal that a continuous B-BSF seed layer with a few residues was

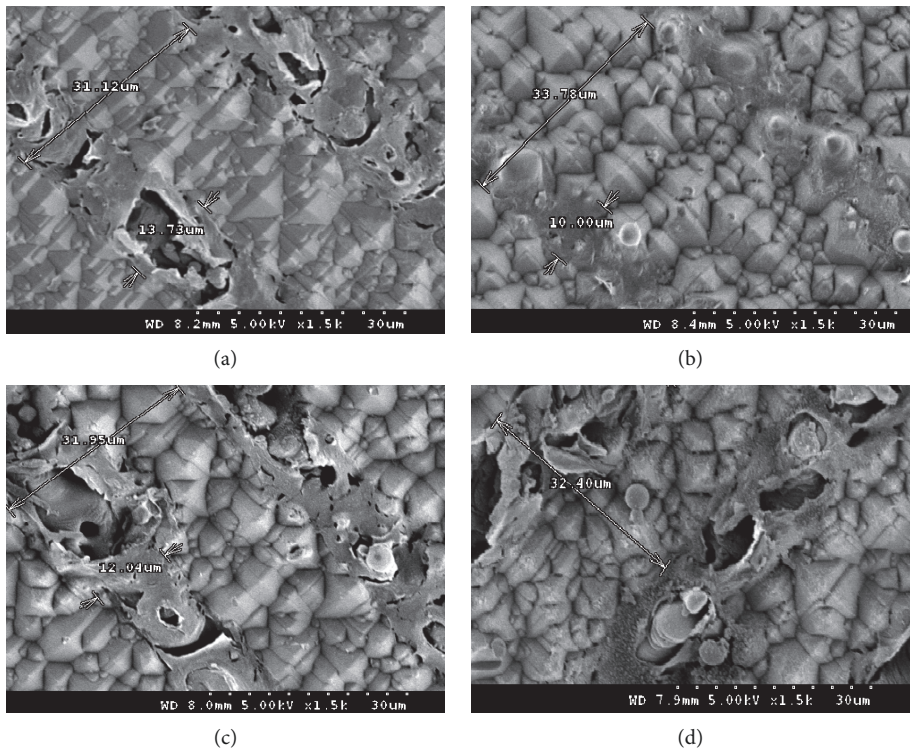

Figure 3: FESEM surface morphology images of backside surfaces of SPMSCs with various laser powers of (a) 0.8, (b) 1.0, (c) 1.2, and (d) 1.4 W.

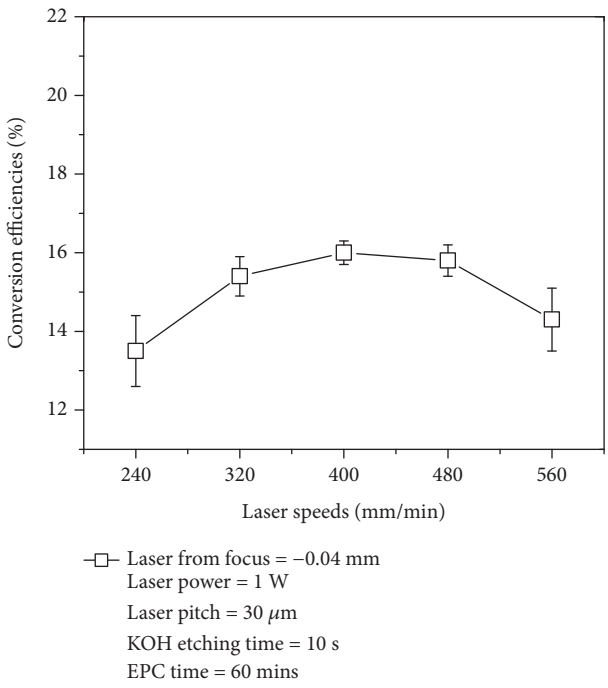

Figure 4: Conversion efficiency vs. laser speed curve of SPMSCs with a B-BSF seed layer and EPC contact layer as the rear contacts.

presented at a KOH etching time of 30 s, as shown in Figure 9(a). However, an increase of the laser groove in the B-BSF seed layer region was addressed at a KOH treatment of 40 s, as shown in Figure 9(b). A broken B-BSF seed layer could be formed at a long KOH etching time. Thus, a suitable KOH etching time should help in the formation of a continuous B-BSF seed layer with low laser damage. A suitable KOH etching time was presented below 30 s in this work.

To investigate the effects of various EPC times on the conversion efficiencies of SPMSCs with a B-BSF seed layer and EPC contact layer as the rear contacts, the conversion efficiency vs. EPC time curve is shown in Figure 10(a). The results show that the conversion efficiency degradations were presented at both short and long EPC times. The thickness of EPC formed at 40 min was measured to be approximately 50 μm, as shown in Figure 10(b). The achievement of a conversion efficiency improvement of more than 1.7% absolute from 15.4% to 17.1% for SPMSCs with a tuning EPC time was explored.

Figure 11 shows various FESEM surface morphology images of the backside surfaces of SPMSCs with various EPC times of (a) 20, (b) 30, (c) 40, and (d) 50 min. It can be seen that a broken EPC contact layer was presented below 30 min, as shown in Figure 11(a). The spacing of the EPC contact layer decreases with increasing EPC time. A continuous EPC contact layer was addressed at an EPC time of 40 min, as shown in Figure 11(c). Furthermore, a thicker EPC contact layer was formed up to 50 min, as shown in

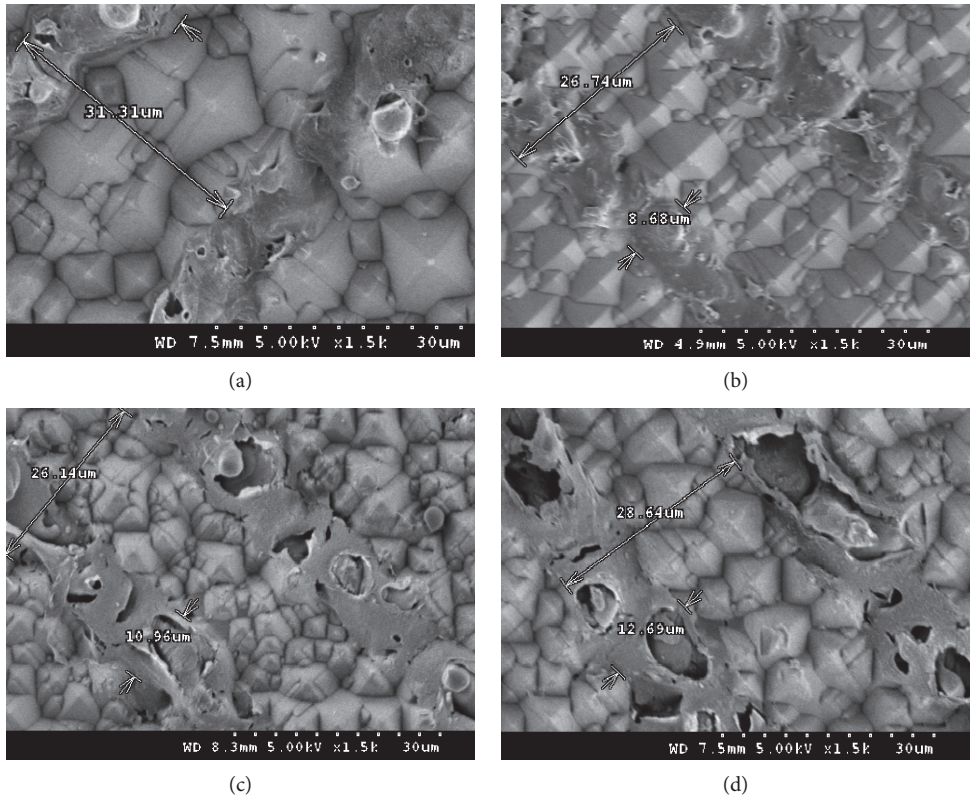

Figure 5: FESEM surface morphology images of backside surfaces of SPMSCs with various laser speeds of (a) 320, (b) 400, (c) 480, and (d) 560 mm/min.

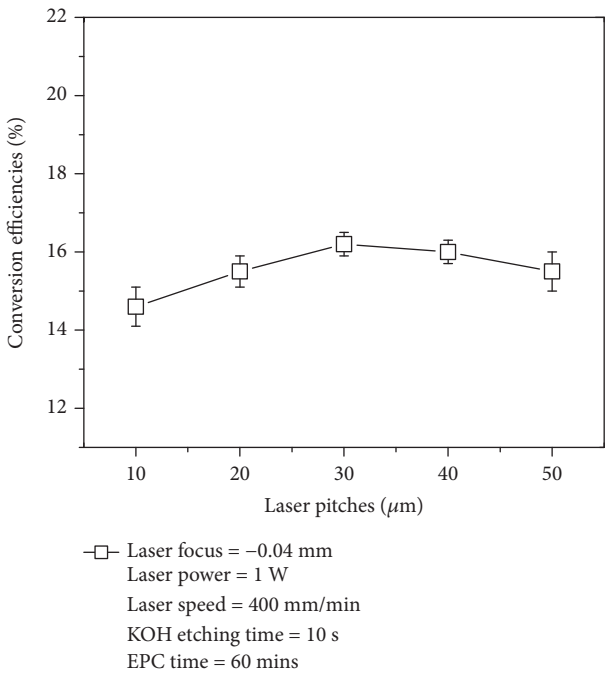

Figure 6: Conversion efficiency vs. laser line pitch curve of SPMSCs with a B-BSF seed layer and EPC contact layer as the rear contacts.

Figure 11(d). A thicker EPC contact layer was demonstrated at a high EPC time resulting in a large series resistance [13]. Moreover, an excellent resistivity caused by the Cu crystal orientation of (111) was demonstrated for the EPC formed at a current density of 25 mA/cm^2 [13]. The reason can be attributed to the (111)-oriented copper film with no slip line [24]. Thus, a suitable EPC time was demonstrated at 40 min in this work.

To increase the adhesion between the B-BSF seed layer and EPC contact layer, a laser pinhole process after the LD process was proposed. Afterwards, a KOH etching time of 30 s was addressed. The width and depth of a laser pinhole were measured to be approximately 14.85 and 9.9 μm, respectively, as shown in Figure 12(a). The current density vs. gate voltage curves of SPMSCs with and without laser pinhole processes are shown in Figure 12(b). In general, a screen-printed Al rear was used as rear contacts for SPMSCs [7]. Thus, the current density vs. gate voltage curve of a SPMSC with a screen-printed Al rear was used as a reference. The results suggest that a laser pinhole process helps in the improvement of conversion efficiency. Compared with the SPMSCs without a laser pinhole process, the achievement of a conversion efficiency improvement of more than 0.6% absolute from 17.1% to 17.7% for SPMSCs with a laser pinhole process was explored. Furthermore, compared with the SPMSCs with a screen-printed Al rear, the achievement of a conversion efficiency improvement of more than 1.5%

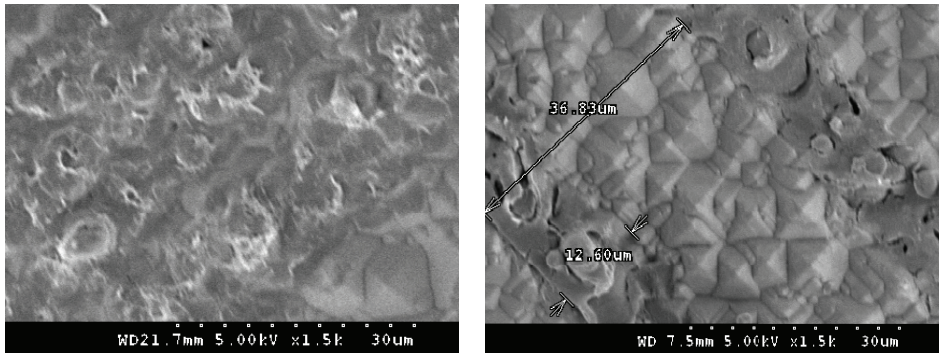

(a) (b)

Figure 7: FESEM surface morphology images of backside surfaces of SPMSCs with various laser line pitches of (a) 10 and (b) 40 μm.

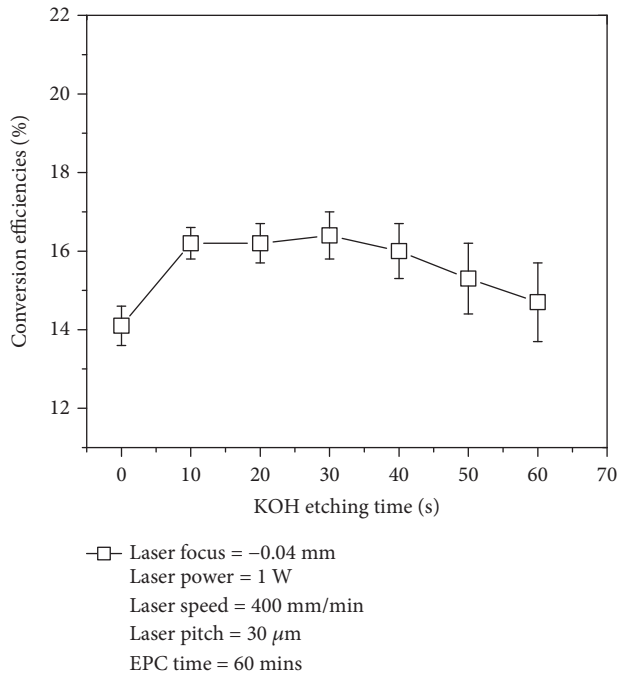

Figure 8: Conversion efficiency vs. KOH etching time curve of SPMSCs with a B-BSF seed layer and EPC contact layer as the rear contacts.

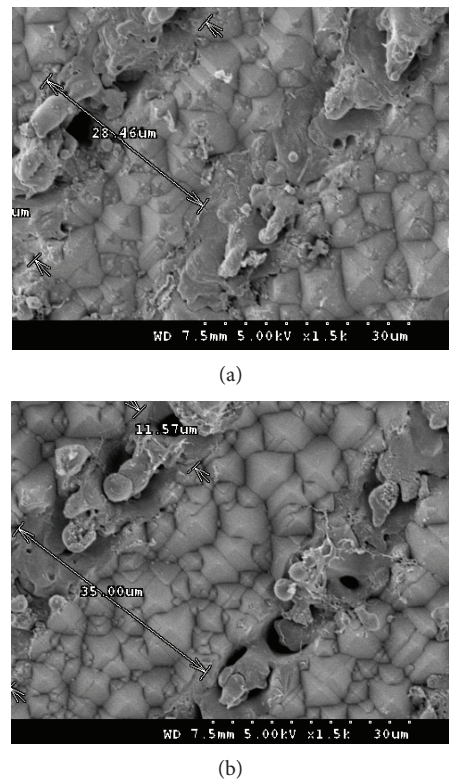

(a) (b)

Figure 9: FESEM surface morphology images of backside surfaces of SPMSCs with various KOH etching times of (a) 30 and (b) 40 s.

absolute from 16.2% to 17.7% for SPMSCs with a laser pinhole process was demonstrated. One method to evaluate the series resistance from a solar cell is to find the slope of the J-V curve at the open-circuit voltage point [13]. The series resistances of 0.4 and 0.6 $\Omega\cdot cm^2$ for SPMSCs with EPC and screen-printed Al as the rear contacts, respectively, were demonstrated. Thus, EPC techniques possess a potential to enhance the series resistance of SPMSCs. Moreover, the open-circuit voltages of 633 and 614 mV for SPMSCs with EPC and screen-printed Al as the rear contacts, respectively, were achieved, as shown in Figure 12(b). The rear surface recombination velocities ranging from 200 to 450 cm/s were provided by an Al back surface field [25, 26]. Therefore, a B-BSF is better than an Al back surface field for surface passivation.

To estimate the adhesion between the B-BSF seed layer and EPC contact layer, various peeling force profiles of SPMSCs with and without a laser pinhole are shown in Figure 13. In general, a screen-printed Ag rear was used as an interconnection for the silicon module [27, 28]. Thus, a peeling force profile of a SPMSC with a screen-printed Ag rear was used as a reference. The peeling force profile of a SPMSC with laser pinhole posttreatment was better than that without laser pinhole posttreatment. An adhesion of up to 2 N/mm was demonstrated by SPMSCs with laser pinhole posttreatment. Compared with the SPMSCs without laser pinhole posttreatment, an enhanced adhesion of 1.36 N/mm was achieved for the SPMSCs with laser pinhole

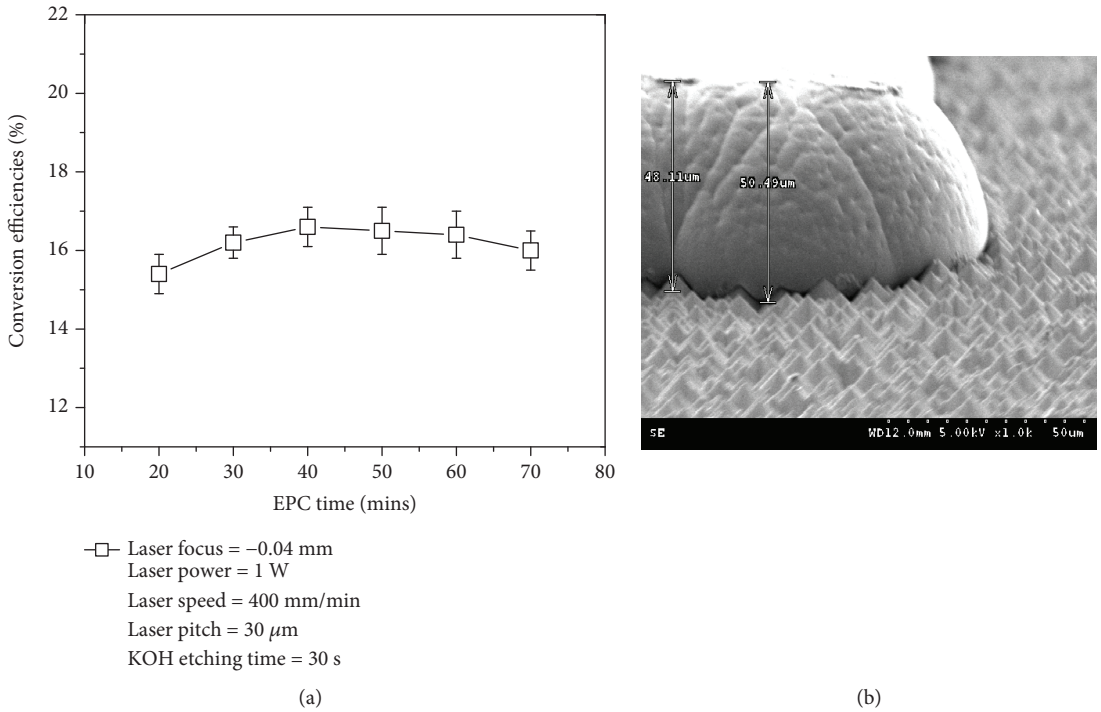

(a) (b)

Figure 10: (a) Conversion efficiency vs. EPC time curve of SPMSCs with a B-BSF seed layer and EPC contact layer as the rear contacts. (b) FESEM surface morphology images of backside surfaces of SPMSCs with an EPC time of 40 min.

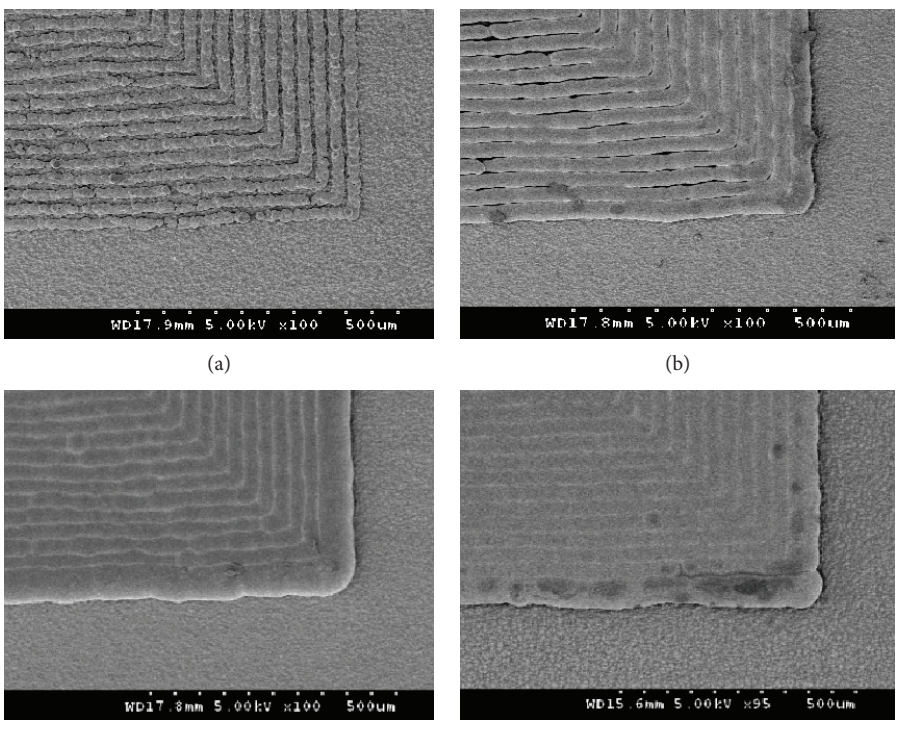

(a) (b)

(c) (d)

Figure 11: FESEM surface morphology images of backside surfaces of SPMSCs with various EPC times of (a) 20, (b) 30, (c) 40, and (d) 50 min.

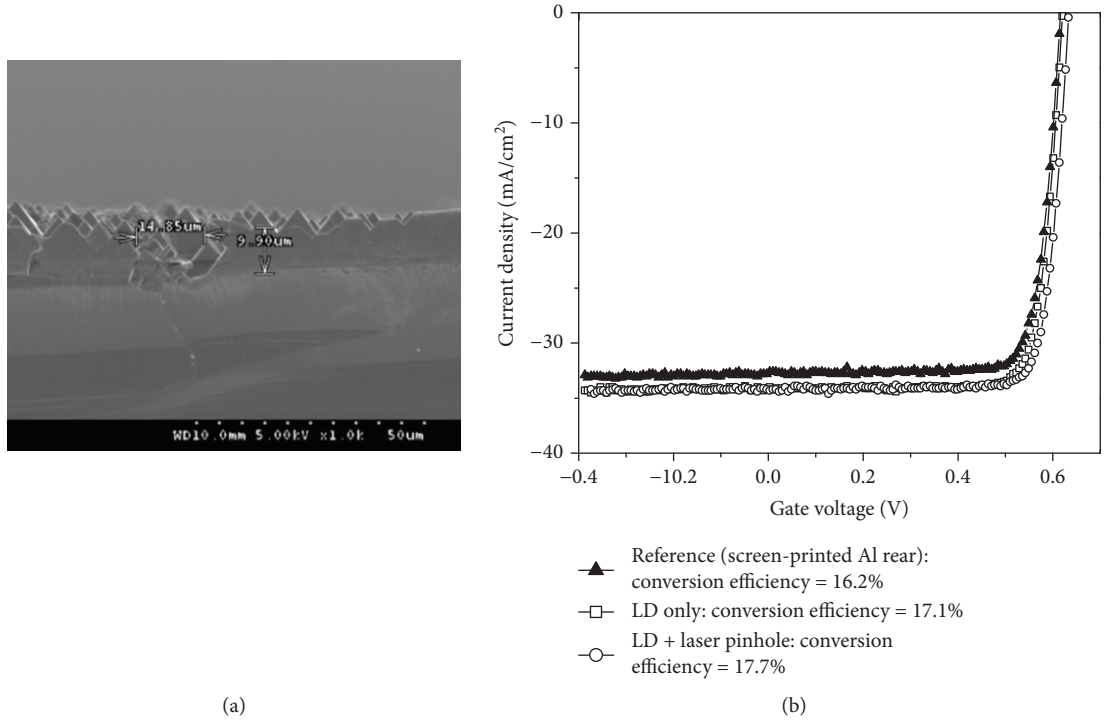

Figure 12: (a) FESEM cross-sectional image of the backside of SPMSCs with a laser pinhole process. (b) Current density vs. gate voltage curve of SPMSCs with and without laser pinhole processes is shown.

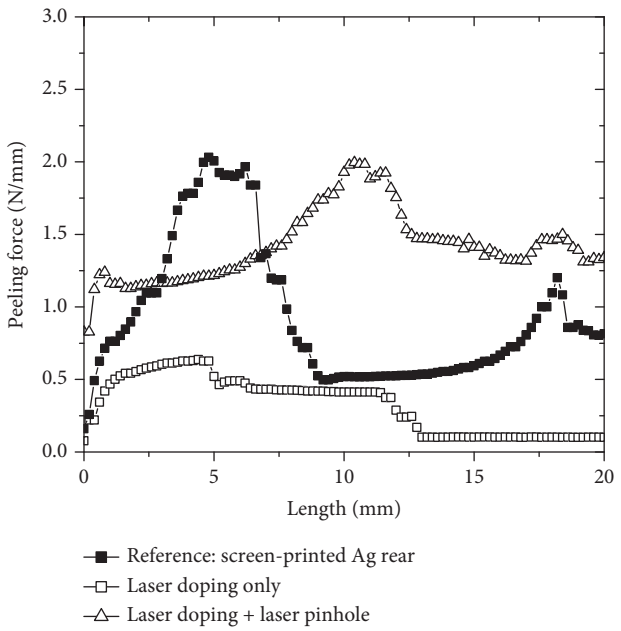

Figure 13: Peeling force profiles of SPMSCs with a B-BSF seed layer and EPC contact layer as the rear contacts. A peeling force profile of a SPMSC with a screen-printed Ag rear was used as a reference.

posttreatment. It has been reported that a peeling force of 1–5 N/mm for a laser spot soldering technique was demonstrated [29]. Thus, to promote the adhesion between the B-BSF seed layer and EPC contact layer, a laser pinhole posttreatment was proposed after the LD process. An adhesion of up to 2 N/mm for the SPMSCs with laser pinhole posttreatment was similar to that of SPMSCs with a screen-printed Ag rear.

4. Conclusions

A suitable LD process was presented for the improvement of the conversion efficiencies of SPMSCs with the B-BSF seed layer and EPC contact layer as the rear contacts. A continuous B-BSF seed layer was demonstrated at −0.04 mm from the laser focus, with a laser power of 1 W, laser speed of 400 mm/min, laser line pitch of 30 μm, and KOH etching time of 30 s after the LD process. Excellent adhesion of up to 2.0 N/mm was demonstrated by a laser pinhole process. Compared with the SPMSCs with a screen-printed Al rear, the achievement of a conversion efficiency improvement of more than 1.5% absolute from 16.2% to 17.7% for SPMSCs with EPC as the rear contact was explored.

Data Availability

The data used to support the findings of this study are available from the corresponding author upon request.

Conflicts of Interest

The authors declare that they have no conflicts of interest.

Acknowledgments

The authors would like to thank the Ministry of Science and Technology in Taiwan for the financial support under contract number MOST 107-2221-E-150-049. We thank Futurrex Inc. and Wellspring & Vim Tech. Corp. for supporting spin-on doping technology.

References

[1] E. Lee, K. Cho, D. Oh et al., "Exceeding 19% efficient 6 inch screen printed crystalline silicon solar cells with selective emitter," *Renewable Energy*, vol. 42, pp. 95–98, 2012.

[2] T. Y. Kwon, D. H. Yang, M. K. Ju et al., "Screen printed phosphorus diffusion for low-cost and simplified industrial mono-crystalline silicon solar cells," *Solar Energy Materials and Solar Cells*, vol. 95, no. 1, pp. 14–17, 2011.

[3] M. M. Hilali, J. M. Gee, and P. Hacke, "Bow in screen-printed back-contact industrial silicon solar cells," *Solar Energy Materials and Solar Cells*, vol. 91, no. 13, pp. 1228–1233, 2007.

[4] D. H. Neuhaus and A. Munzer, "Industrial silicon wafer solar cells," *Advances in OptoElectronics*, vol. 2007, Article ID 24521, 15 pages, 2007.

[5] S. Riegel, F. Mutter, T. Lauermann, B. Terheiden, and G. Hahn, "Review on screen printed metallization on p-type silicon," *Energy Procedia*, vol. 21, pp. 14–23, 2012.

[6] C. Kranz, U. Baumann, B. Wolpensinger et al., "Void formation in screen-printed local aluminum contacts modeled by surface energy minimization," *Solar Energy Materials and Solar Cells*, vol. 158, pp. 11–18, 2016.

[7] Y. S. Chiu, C. L. Cheng, T. J. Whang, and G. Y. Ji, "Effects of silicate glasses in aluminum pastes on physical and electrical characteristics of screen-printed multi-crystalline silicon solar cells," *Materials Letters*, vol. 126, pp. 143–146, 2014.

[8] M. A. Green, *Third Generation Photovoltaics: Advanced Solar Energy Conversion*, Springer, 2006.

[9] A. Bouyelfane and A. Zerga, "Ni/Cu electroplating, a worthwhile alternative to use instead of Ag screen-printed front side metallization of conventional solar cells," *Materials Science in Semiconductor Processing*, vol. 26, pp. 312–319, 2014.

[10] J. D. Lee, H. Y. Kwon, M. J. Kim, E. J. Lee, H. S. Lee, and S. H. Lee, "The investigation of one step annealing for plated Ni/Cu contact solar cells," *Renewable Energy*, vol. 42, pp. 1–3, 2012.

[11] A. Ebong, "Pathway to low-cost metallization of silicon solar cell through understanding of the silicon metal interface and plating chemistry," *Electrochimica Acta*, vol. 128, pp. 336–340, 2014.

[12] S. Kluska, C. Fleischmann, A. Büchler et al., "Micro characterization of laser structured solar cells with plated Ni–Ag contacts," *Solar Energy Materials and Solar Cells*, vol. 120, pp. 323–331, 2014.

[13] C. C. Liu, C. L. Cheng, J. S. Siao, and G. M. Hong, "Enhanced photovoltaic characteristics of screen-printed monocrystalline silicon solar cells by rear electroplated copper," *ECS Journal of Solid State Science and Technology*, vol. 6, no. 8, pp. P561–P565, 2017.

[14] L. Tous, R. Russell, J. Das et al., "Large area copper plated silicon solar cell exceeding 19.5% efficiency," *Energy Procedia*, vol. 21, pp. 58–65, 2012.

[15] W. J. Oh and S. H. Lee, "Investigation of selective emitter in single step diffusion process for plated Ni/Cu metallization crystalline silicon solar cells," *Current Applied Physics*, vol. 13, pp. S186–S189, 2013.

[16] Z. Hameiri, L. Mai, T. Puzzer, and S. R. Wenham, "Influence of laser power on the properties of laser doped solar cells," *Solar Energy Materials and Solar Cells*, vol. 95, no. 4, pp. 1085–1094, 2011.

[17] C. L. Cheng, C. T. Yeh, and C. C. Liu, "Study on laser doping and electroplating copper for monocrystalline silicon solar cell applications," in *192nd International Conference on Science, Technology, Engineering and Management*, p. 3491, Tokyo, Japan, 2017.

[18] Z. R. Du, N. Palina, J. Chen, A. G. Aberle, B. Hoex, and M. H. Hong, "Enhancement of laser-induced rear surface spallation by pyramid textured structures on silicon wafer solar cells," *Optics Express*, vol. 20, no. S6, pp. A984–A990, 2012.

[19] S. Eisele, T. Roder, M. Ametowobla, G. Bilger, J. R. Kohler, and J. H. Werner, "18.9% efficient silicon solar cell with laser doped emitter," in *2009 34th IEEE Photovoltaic Specialists Conference (PVSC)*, pp. 883–885, Philadelphia, PA, USA, 2009.

[20] M. Kim, D. Kim, D. Kim, and Y. Kang, "Analysis of laser-induced damage during laser ablation process using picosecond pulse width laser to fabricate highly efficient PERC cells," *Solar Energy*, vol. 108, pp. 101–106, 2014.

[21] M. Kim, S. Park, and D. Kim, "Highly efficient PERC cells fabricated using the low cost laser ablation process," *Solar Energy Materials and Solar Cells*, vol. 117, pp. 126–131, 2013.

[22] K. S. Wang, B. S. Tjahjono, J. Wong, A. Uddin, and S. R. Wenham, "Sheet resistance characterization of laser-doped lines on crystalline silicon wafers for photovoltaic applications," *Solar Energy Materials and Solar Cells*, vol. 95, no. 3, pp. 974–980, 2011.

[23] J. Kim, Y. Hwang, J. Kim, J. Lim, and E. Lee, "Investigation of rear side selective laser ablation and damage etching process for industrial PERC solar cells," *Energy Procedia*, vol. 55, pp. 791–796, 2014.

[24] A. F. Burnett and J. M. Cech, "Relationship of crystallographic orientation and impurities to stress, resistivity, and morphology for sputtered copper films," *Journal of Vacuum Science and Technology A*, vol. 11, no. 6, pp. 2970–2974, 1993.

[25] S. Narasimha and A. Rohatgi, "Optimized aluminum back surface field techniques for silicon solar cells," in *Conference Record of the Twenty Sixth IEEE Photovoltaic Specialists Conference - 1997*, pp. 63–66, Anaheim, CA, USA, 1997.

[26] T. Dullweber, S. Gatz, H. Hannebauer et al., "Towards 20% efficient large-area screen-printed rear-passivated silicon solar cells," *Progress in Photovoltaics: Research and Applications*, vol. 20, no. 6, pp. 630–638, 2012.

[27] M. T. Zarmai, N. N. Ekere, C. F. Oduoza, and E. H. Amalu, "A review of interconnection technologies for improved crystalline silicon solar cell photovoltaic module assembly," *Applied Energy*, vol. 154, pp. 173–182, 2015.

[28] H. Helmers, E. Oliva, W. Bronner, F. Dimroth, and A. W. Bett, "Processing techniques for monolithic interconnection of solar cells at wafer level," *IEEE Transactions on Electron Devices*, vol. 57, no. 12, pp. 3355–3360, 2010.

[29] H. Schmidhuber, S. Klappert, J. Stollhof, G. Erfurt, M. Eberspächer, and R. Preu, "Laser soldering—a technology for better contacts," in *20th European Photovoltaic Solar Energy Conference*, pp. 1–4, Barcelona, Spain, 2005.